Naval Research Laboratory
Washington, DC 20375-5320

NRL/6930/MR—2022/2

Dynamic Plasmonic Optics in Dense Nanorod Phases

NICHOLAS J. GREYBUSH

Laboratory for Bio/Nano Science and Technology Branch
Center for Bio/Molecular Science and Engineering Division

February 10, 2022

REPORT DOCUMENTATION PAGE

Form Approved
OMB No. 0704-0188

1. REPORT DATE *(DD-MM-YYYY)*
10-02-2022

2. REPORT TYPE
NRL Memorandum Report

3. DATES COVERED *(From - To)*
20 July 2020 – 19 July 2021

4. TITLE AND SUBTITLE
Dynamic Plasmonic Optics in Dense Nanorod Phases

5a. CONTRACT NUMBER

5b. GRANT NUMBER

5c. PROGRAM ELEMENT NUMBER
NISE

6. AUTHOR(S)
Nicholas J. Greybush

5d. PROJECT NUMBER

5e. TASK NUMBER

5f. WORK UNIT NUMBER
N2X8

7. PERFORMING ORGANIZATION NAME(S) AND ADDRESS(ES)

Naval Research Laboratory
4555 Overlook Avenue, SW
Washington, DC 20375-5320

8. PERFORMING ORGANIZATION REPORT NUMBER
NRL/6930/MR--2022/2

9. SPONSORING / MONITORING AGENCY NAME(S) AND ADDRESS(ES)

Naval Research Laboratory
4555 Overlook Avenue, SW
Washington, DC 20375-5320

10. SPONSOR / MONITOR'S ACRONYM(S)
NRL-NISE

11. SPONSOR / MONITOR'S REPORT NUMBER(S)

12. DISTRIBUTION / AVAILABILITY STATEMENT

DISTRIBUTION STATEMENT A: Approved for public release; distribution is unlimited.

13. SUPPLEMENTARY NOTES
Karles Fellowship

14. ABSTRACT

Metal plasmonic nanorods (NRs) both interact strongly with light and can be aligned by an external electric field, presenting a new paradigm for displays and high-speed optical devices. While the utility of these materials has been clearly forecasted, the limits of their performance have formerly remained untested. We now demonstrate highly dense NR suspensions and map NR alignment at concentrations across several orders of magnitude. First, we refine organic ligand and solvent chemistry to achieve stable Au NR suspensions. We fabricate custom plasmonic pixel cells with precise optical path lengths and directly measure the pixels' exceptional optical densities in a lab-designed apparatus incorporating laser illumination and high-sensitivity detectors. We apply alternating current electric fields to the pixels, rapidly inducing orientational order among the NRs, resulting in a large contrast in transmitted optical power. By formulating, understanding, and controlling highly concentrated and optically dense plasmonic NR suspensions, we begin to exploit their properties for dynamic optoelectronic applications.

15. SUBJECT TERMS

16. SECURITY CLASSIFICATION OF:			**17. LIMITATION OF ABSTRACT**	**18. NUMBER OF PAGES**	**19a. NAME OF RESPONSIBLE PERSON**
a. REPORT	**b. ABSTRACT**	**c. THIS PAGE**			Nicholas J. Greybush
U	U	U	U	21	**19b. TELEPHONE NUMBER** *(include area code)* (202) 404-6123

Standard Form 298 (Rev. 8-98)
Prescribed by ANSI Std. Z39.18

This page intentionally left blank.

CONTENTS

INTRODUCTION 1

EXPERIMENTAL METHODS 1
    Nanorod Synthesis and Preparation 1
        Materials 1
        Synthesis 1
        Purification 2
        Phase Transfer 2
    Nanorod Structural Characterization 3
    Pixel Fabrication 3
        Substrate Preparation 3
        Pixel Assembly 3
        Pixel Wiring 3
        Pixel Filling 4
    Pixel Control 4
    Optical Characterization 4

RESULTS AND DISCUSSION 4

CONCLUSIONS 15

RELATED PUBLICATIONS 15

ACKNOWLEDGEMENTS 15

REFERENCES 15

FIGURES

Fig. 1 — Absorption spectrum of Au nanorods (NRs) in hydrogenated terphenyl (HTP) when the NRs are randomly oriented (“unaligned”) and when aligned by an external electric field (“aligned”)...................... 5

Fig. 2 — Representative transmission electron microscope (TEM) images of Au NRs (a) before and (b) after functionalization with polystyrene-thiol and phase transfer to toluene... 5

Fig. 3 — (a) Drawing (dimensions in mm) of a pixel cell. Green regions represent areas from which the indium tin oxide (ITO) coating is to be removed. (b) Photograph of a pixel cell loaded with HTP............ 6

Fig. 4 — Schematic depiction of Au NR alignment under the application of an electric field. Incident light excites longitudinal surface plasmon (LSP) and transverse surface plasmon (TSP) resonances in the NRs. 6

Fig. 5 — Photographs as a function of applied electric field of a 1064 nm laser shining through a Au NR pixel and incident on a ground glass diffuser. The images were acquired by a digital camera through a 695 nm long pass filter.. 7

Fig. 6 — Photograph of apparatus constructed for measurement of Au NR pixels’ absorption at 1064 nm 7

Fig. 7 — Representative measured absorbance at 1064 nm of Au NRs in a pixel cell as a function of applied electric field (E-field). The optical path length in this example is 100 µm, and the applied E-field is estimated by dividing the applied voltage by the distance between the ITO electrodes. 8

Fig. 8 — Measured absorption at 1064 nm of Au NRs in pixel cells with an optical path of 100 µm as a function of applied voltage (bottom scale) or E-field (top scale). The 1 cm equivalent absorbance (right scale) indicates the absorbance that the NR suspensions in the pixels would have at an optical path of 1 cm. Labels of “OD01–10” indicate nominal optical density targets and represent NR samples prepared with increasing concentrations.. 9

Fig. 9 — Absorbance values at the indicated applied voltage levels extracted from the data of Fig. 8. “Nominal OD” indicates target values used in preparation of the NR suspensions and directly relates to NR concentration. The lines are provided as guides to the eye. 10

Fig. 10 — Alignment of Au NRs in pixels with optical path lengths of (a) 100 (b) 50 (c) 25 and (d) 10 µm. Individual data sets with unique symbols represent pixels prepared with different concentrations.... 11

Fig. 11 — (a) Alignment responses of all of the NR pixels (100, 50, 25, and 10 µm paths) from Fig. 10 combined into a single plot expressed in terms of 1 cm equivalent absorbance and geometrically calculated applied electric field strength. (b) Data from (a) where each set is normalized by dividing by its maximum absorbance. 12

Fig. 12 — (a) Maximum value of the scalar order parameter *S* and (b) value of the critical electric field for alignment E_c extracted from alignment data from pixels with the indicated path lengths (in µm) as a function of the maximum 1 cm equivalent absorbance of the pixel. (c) Average maximum *S* and (d) average E_c for each optical path length, with error bars representing one standard deviation................... 13

Fig. 13 — (a) Absorbance and (b) transmittance contrast ratio for pixels with the indicated path lengths (in µm) as a function of the maximum 1 cm equivalent absorbance of the pixel 14

EXECUTIVE SUMMARY

This report presents research conducted by Nicholas J. Greybush under the Jerome and Isabella Karle Distinguished Scholar Fellowship Program (20 July 2020 – 19 July 2021).

The objective of this research program was to formulate, understand, and control highly concentrated and optically dense plasmonic nanorod phases, and to exploit their properties for dynamic optoelectronic devices.

This page intentionally left blank.

DYNAMIC PLASMONIC OPTICS IN DENSE NANOROD PHASES

INTRODUCTION

Metal plasmonic nanorods (NRs) both interact strongly with light and can be aligned by an external electric field,[1] presenting a new paradigm for displays and high-speed optical devices.[2–4] While the utility of these materials has been clearly forecasted,[5] the limits of their performance have formerly remained untested. We now demonstrate highly dense NR suspensions and map NR alignment at concentrations across several orders of magnitude. First, we refine organic ligand and solvent chemistry to achieve stable Au NR suspensions. We fabricate custom plasmonic pixel cells with precise optical path lengths and directly measure the pixels' exceptional optical densities in a lab-designed apparatus incorporating laser illumination and high-sensitivity detectors. We apply alternating current (AC) electric fields to the pixels, rapidly inducing orientational order among the NRs, resulting in a large contrast in transmitted optical power. By formulating, understanding, and controlling highly concentrated and optically dense plasmonic NR suspensions, we begin to exploit their properties for dynamic optoelectronic applications.

EXPERIMENTAL METHODS

Nanorod Synthesis and Preparation

Materials

Hexadecyltrimethylammonium bromide (CTAB, 98%) was purchased from GFS Chemicals. Benzyldimethylhexadecylammonium chloride (BDAC) was purchased from TCI America. $HAuCl_4$, $AgNO_3$, hydroquinone, sodium borohydride, and L-ascorbic acid were purchased from Aldrich. Tetrahydrofuran (THF, HPLC grade), toluene (HPLC grade), and 2-propanol (ACS Plus grade) were purchased from Fisher Scientific. Thiol-terminated polystyrene (PS-thiol, $M_n = 31{,}000$) was purchased from Polymer Source, Inc. Hydrogenated terphenyl (HTP) was purchased from Alfa Chemistry.

Synthesis

A Au seed solution was prepared according to the typical synthetic route.[6,7] $HAuCl_4$ (0.025 mL, 0.1 M) was added to an aqueous solution of CTAB (10 mL, 0.1 M). A freshly prepared, $NaBH_4$ solution (0.6 mL, 0.01 M) was kept in the refrigerator (3 °C) for 5 min. It was then added into the mixture under vigorous stirring (2 min.). The color of the solution instantly became light brown. The seed solution was aged for 10 min. before being added into the growth solution.

Two growth solutions ("A" and "B") were prepared according to the following procedure.[8] The growth solution A was prepared by mixing $HAuCl_4$ (0.25 mL, 0.1 M), $AgNO_3$ (0.25 mL, 0.1 M), and CTAB (50 mL, 0.1 M) followed by the addition of hydroquinone solution (1.25 mL, 0.1 M) as a reducing agent. When the solution became clear (~10 min.), diluted HCl solution (0.18 mL, 1 M) was added. Finally, 5 mL of the Au seed solution was added with gentle shaking of the flask. The as-prepared solution was left at 25 °C for 24 h. BDAC (2 g) was then added, and the mixture was left at 25 °C for 30 min.

Manuscript approved February 2, 2022.

The growth solution B was prepared by mixing $HAuCl_4$ (2.5 mL, 0.1 M), $AgNO_3$ (0.4 mL, 0.1 M), CTAB (0.9 g) and BDAC (1.1 g) in 85 mL of water. Hydroquinone solution (12.5 mL, 0.1 M) was then added. The as-made solution was kept at 25 °C for 10 min.

The two growth solutions A and B were mixed together and left inside an oven at 25 °C for 24 h.

Purification

Before further purification, the temperature of the NR suspension was raised to 30 °C in a water bath to dissolve any crystallized surfactant. Warm (~35 °C) 18 MΩ deionized (DI) water (EMD Millipore Milli-Q Advantage A10) was added to the approximately 156 mL of as-synthesized NR suspension to bring the volume to 240 mL, and the resulting suspension was divided among six centrifuge tubes (50 mL Thermo Scientific Nunc). The six tubes were processed identically according to the following steps. Excess surfactant was removed by centrifuging at 5000 rpm (4304 ×*g*), 30 °C for 1 h (Thermo Scientific Sorvall Lynx 4000 centrifuge with Fiberlite F14-14×50cy rotor). The supernatant was decanted with a serological pipette and discarded, and the precipitate was redispersed with 40 mL warm DI water. The sample was then vortexed for 10 s to aid redispersion. The sample was centrifuged a second time under the same conditions; the supernatant was decanted and discarded, and the precipitate was redispersed with 35 mL warm DI water then vortexed.

Nanocrystals with non-rod shapes were removed through further purification. Addition of a NaCl solution resulted in selective precipitation of the desired NRs, enabling removal of the undesired byproducts.[9] Specifically, 5 mL of 1.5 M NaCl was added to the 35 mL NR suspension, followed by 10 s vortexing. The sample was left undisturbed for ~18 h at 25–28 °C to allow the NRs to flocculate and settle into a visible pellet. The magenta-colored supernatant was decanted and discarded, and the precipitated NRs were redispersed in 50 µL of 1.1 mM CTAB. 5 mL of warm DI water was added, and the sample was vortexed for 10 s.

Phase Transfer

The Au NRs were then phase-transferred from aqueous to non-polar solvents by functionalizing the NRs with PS-thiol.[1,2] The six 5 mL samples prepared above were combined into three 10 mL volumes that were each placed in a 30 mL glass vial and processed identically as follows. To 5 mL of THF, 0.05 g PS-thiol was added and dissolved. The PS-thiol/THF solution was added to the 10 mL Au NRs, and the vial was capped and shaken for 1 min. The Au NRs formed flocculates on the side of the vial and in the liquid, which were allowed to settle to the bottom of the vial for 20 min. The colorless solvent was then decanted and discarded, and any remaining solvent was evaporated with the flow of dry N_2. The PS-thiol-functionalized Au NRs were redispersed in 10 mL of toluene.

The Au NRs were then purified from excess, unbound PS-thiol. To promote precipitation during centrifugation, 5 mL of 2-propanol was added to 10 mL of Au NR suspension in toluene, followed by vortexing for 30 s. The sample was centrifuged at 9000 rpm (13,945 ×g), 30 °C for 1 h; the supernatant was decanted and discarded, and the precipitate was redispersed with toluene to 30 mL. 10 mL of 2-propanol was added, followed by vortexing for 30 s. The sample was centrifuged a second time at 9000 rpm, 30 °C for 1 h; the supernatant was decanted and discarded, and the precipitate was redispersed with toluene to 30 mL. 10 mL of 2-propanol was added, followed by vortexing for 30 s. The sample was centrifuged a third time at 9000 rpm, 30 °C for 1 h; the supernatant was decanted and discarded, and the precipitate was redispersed with toluene to the desired Au NR concentration.

The Au NRs were then transferred from toluene to HTP. The desired final volume of HTP was dispensed into a 0.5 mL microcentrifuge tube. A volume of Au NR suspension in toluene, the amount determined by the desired final Au NR concentration, was dispensed into the tube with the HTP. The Au NRs in toluene initially remained a separate phase atop the HTP in the bottom of the tube. The uncapped tube was placed in a 20 mL glass scintillation vial and placed under dry N_2 flow for ~48 h to evaporate the toluene, leaving behind Au NRs dispersed in HTP.

Nanorod Structural Characterization

Transmission electron microscopy (TEM) was performed using a JEOL JEM-2200FS field emission electron microscope operating at 200 kV accelerating voltage. Samples were prepared by drop-casting NR suspensions onto holey-carbon-coated TEM grids (SPI Supplies, Structure Probe, Inc.).

Pixel Fabrication

Substrate Preparation

Pixels with customized dimensions and optical paths were fabricated from glass sheets coated on one side with indium tin oxide (ITO, 100 Ω/Sq., 0.33 mm glass thickness, MSE Supplies). The ITO-glass sheets were cut with a 355 nm laser to the desired outer dimensions, and two filling ports were laser cut on half of the sheets to enable loading with NRs. During the cutting stage, the laser's frequency was set to 200 kHz to maximize the power per shot. Then, the ITO within a narrow border around the periphery of the pixel and around the filling ports was removed by laser ablation. During the ITO removal stage, the laser's frequency was set to 500 kHz. Increasing the frequency allowed the laser marking speed to be increased, decreasing the processing time required to remove the ITO. To ensure complete removal, bi-directional hatching with a 5 µm hatch spacing was implemented.

The glass sheets were cleaned by first immersing each sheet in an acetone bath and wiping with a cleanroom wiper. The sheet was then rinsed with a stream of isopropyl alcohol (IPA). Next, the sheet was immersed in an IPA bath and wiped with a cleanroom wiper. The sheet was then rinsed with a stream of IPA and dried with N_2.

Pixel Assembly

The optical path of each pixel was set by introducing spacer beads with well-defined diameters between the two ITO-glass sheets prior to pixel assembly. The spacer beads were obtained from Cospheric LLC with nominal diameters of 100, 50, and 25 µm (spacer grade, soda lime solid glass microspheres) and 10 µm (monodisperse silica microspheres). The spacer beads were loaded into UV-curing optical adhesive (Norland NOA 68T) at 5–10 wt.%. For each pixel, the adhesive was dispensed on the uncoated side of one ITO-glass sheet by a mechanized dispenser in a pattern designed to define a liquid reservoir in the center of the pixel. The second ITO-glass sheet was placed with its uncoated side down upon the first sheet. A weight was applied to the two sheets to spread the adhesive and spacer beads and ensure the spacing between the sheets was minimized to the diameter of the spacers. While weighted, the adhesive was pre-cured with a handheld UV lamp. The pixel was then fully cured by exposure to a large-area, high-intensity UV lamp for 8 min. A post-cure bake was then performed at 50 °C for 12 h.

Pixel Wiring

Electrical control leads were attached to each side of the pixels. Stranded, insulated, 24 AWG wire rated for high voltage (HV) operation (Alpha Wire) was soldered to the ITO-glass of the pixel using an ultrasonic soldering station (S-Bond Technologies, LLC) and indium wire (Sigma-Aldrich) as solder. A thin coating of conductive silver paint (Ted Pella) was applied over the soldered connection and allowed to fully dry.

The electrical connections were then encapsulated with UV-curing epoxy (Norland NOA 91) for added mechanical robustness.

Pixel Filling

Before being filled with Au NR suspensions, the inner reservoir of each pixel was cleaned by flushing with toluene then drying with N_2. Each pixel was filled by dispensing NR suspensions into one of the filling ports and allowing the suspension to be drawn into the pixel by capillary forces. After filling, the ports were sealed with Kapton tape to limit air exposure.

Pixel Control

HV, AC test signals were sent to the pixels from a HV function generator (Vitrek 951i hipot tester) and relay system (Vitrek 964i). The signals were routed using shielded HV wire (Teledyne Reynolds), with the shield grounded to prevent electromagnetic interference. The signals were monitored with a HV probe (Tektronix P6015A) read by an oscilloscope (Tektronix MSO58). Typical test signals were 500 Hz sine waves with peak-to-peak voltages of 0–3 kV applied for 5 s.

Optical Characterization

Visible–near-infrared (Vis–NIR) absorption spectra were obtained using an Ocean Optics QEPro spectrometer and HL-2000, 24 V light source. NIR spectra were also collected with a Bruker Vertex 70V Fourier-transform infrared (FT-IR) spectrometer.

Measurements of optical density at 1064 nm were performed using a custom-designed apparatus. The output of a 1064 nm laser was routed by an optical fiber to a collimating lens then through a beam sampler that directed 10% of the light to an optical power meter (Newport 818-SL head, 1830-C meter) for monitoring the laser output power over time. The main portion of the laser illumination passed through a 2 mm aperture then through a sample holder with 3D-printed inserts designed to hold the pixel cells. The optical power density at the sample surface was estimated at 0.4 W/cm^2. The light transmitted by the sample was collected by an optical power meter head (Ophir PD300R, Ophir Vega meter) outfitted with a 1064 nm bandpass filter to reject stray light. The optical path was enclosed in lens tubes and light-tight covers to minimize noise. Data sampling from the power meters was performed in LabVIEW (National Instruments Corp.). Before measurements were taken, the optical power meters were zeroed with the laser beam blocked. The power measured in the main beamline was continually normalized by the contemporaneously sampled laser power to correct for any fluctuations in laser output.

Photographs of laser light scattered from a ground glass diffuser (Thorlabs) were obtained with a Canon EOS Rebel T3i digital single-lens reflex camera and EF-S 18–55 mm lens. A 695 nm long pass filter was placed in front of the lens to reject the majority of visible light and collect NIR light.

RESULTS AND DISCUSSION

An absorption spectrum of the Au NRs used in the experiments is shown in Fig. 1 (“unaligned”). The longitudinal surface plasmon resonance of the Au NRs after phase transfer is tailored by the synthesis conditions to overlap the common laser wavelength of 1064 nm so that monochromatic absorption measurements over a large dynamic range could be performed. Characterization by transmission electron microscopy (TEM, Fig. 2) illustrates that the typical synthesis produces Au NRs with an average length of 125 ±10 nm and diameter of 17 ±1 nm (N = 25 measurements). While the shell formed by the PS-thiol functionalization of the NRs is not directly visible in the TEM image, an average thickness of at least 10 nm is implied by measuring half the closest distance between NR surfaces in Fig. 2b.

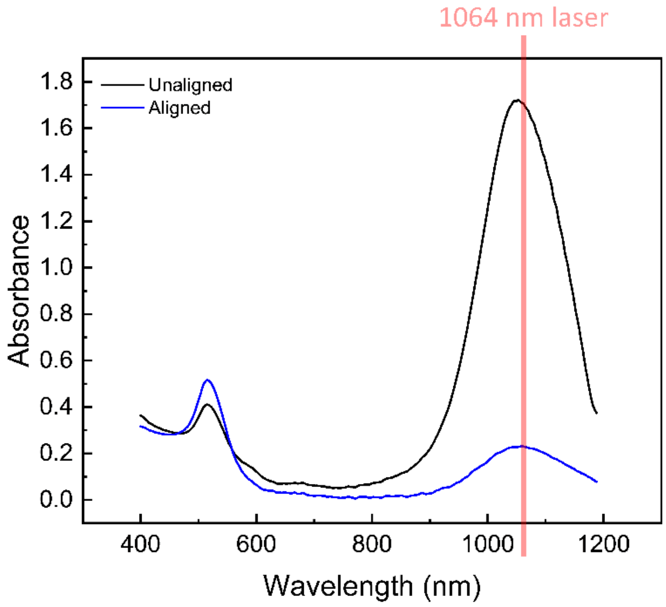

Fig. 1 — Absorption spectrum of Au nanorods (NRs) in hydrogenated terphenyl (HTP) when the NRs are randomly oriented (“unaligned”) and when aligned by an external electric field (“aligned”)

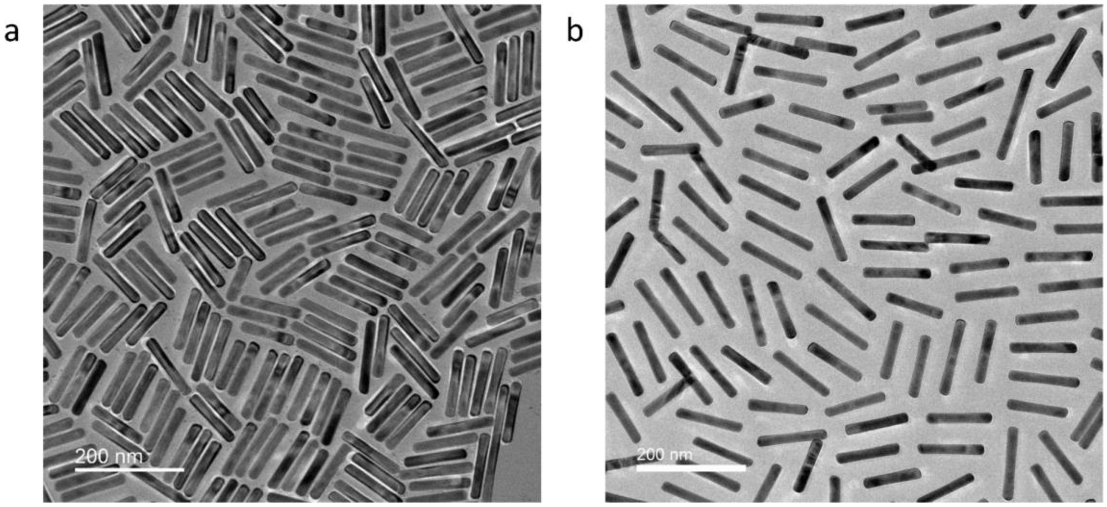

Fig. 2 — Representative transmission electron microscope (TEM) images of Au NRs (a) before and (b) after functionalization with polystyrene-thiol and phase transfer to toluene

Suspensions of Au NRs in HTP are loaded in custom-fabricated pixel cells, a drawing and an example shown in Fig. 3. Application of an AC electric field across the pixel causes the NRs to align, as we have previously demonstrated,[2] and as shown pictorially in Fig. 4. Alignment of the NRs along the direction of light propagation suppresses absorption from the main longitudinal surface plasmon resonance, illustrated in Fig. 1 (“aligned” *vs.* “unaligned”).

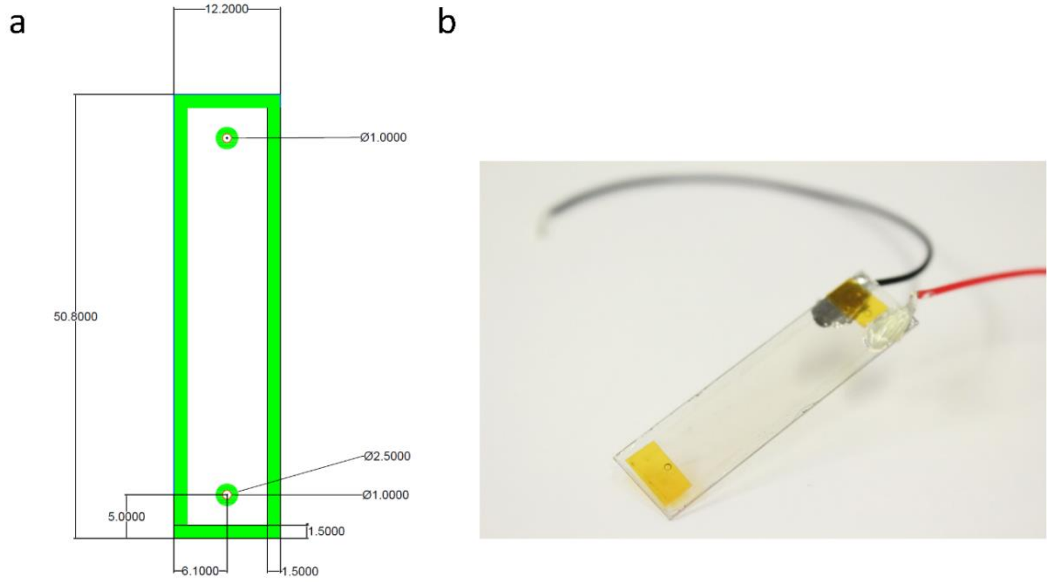

Fig. 3 — (a) Drawing (dimensions in mm) of a pixel cell. Green regions represent areas from which the indium tin oxide (ITO) coating is to be removed. (b) Photograph of a pixel cell loaded with HTP.

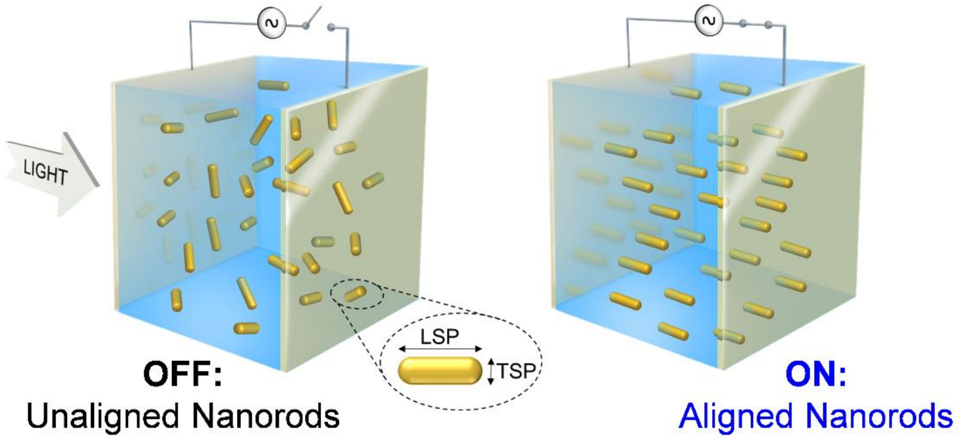

Fig. 4 — Schematic depiction of Au NR alignment under the application of an electric field. Incident light excites longitudinal surface plasmon (LSP) and transverse surface plasmon (TSP) resonances in the NRs.

The reduced absorption at 1064 nm upon NR alignment is visualized in Fig. 5. Laser light passing through a Au NR pixel is imaged as the applied electric field is increased. The increased brightness of the scattered laser light clearly demonstrates that more light passes through the pixel as the NRs are aligned by the electric field. In this manner, the pixels serve as light valves with tunable opacity.

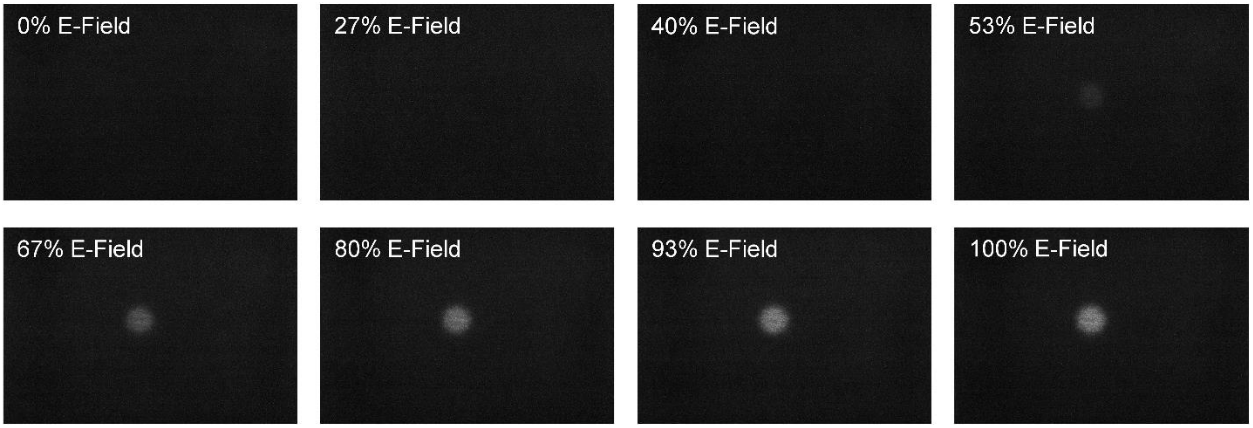

Fig. 5 — Photographs as a function of applied electric field of a 1064 nm laser shining through a Au NR pixel and incident on a ground glass diffuser. The images were acquired by a digital camera through a 695 nm long pass filter.

The quantitative relationship between absorbance (or optical density, OD) and applied electric field is examined by using a custom-built apparatus for absorption measurements at 1064 nm, described in detail in the Experimental Methods section, above, and pictured in Fig. 6. In this context, absorbance is calculated as:

$$Absorbance = -\log_{10} Transmittance = -\log_{10} \frac{I}{I_0} \qquad \text{(Equation 1)}$$

where I is the measured intensity of light passing through a pixel loaded with a Au NR suspension in HTP, and I_0 is the measured intensity of light passing through a pixel loaded with HTP only. In this manner, the absorbance value considers only the contributions of the NRs.

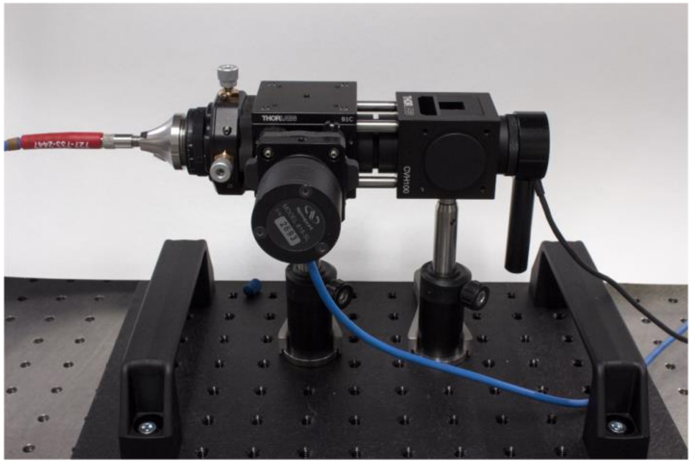

Fig. 6 — Photograph of apparatus constructed for measurement of Au NR pixels' absorption at 1064 nm

The typical response of the absorption of the Au NR suspensions to an applied electric field is demonstrated in Fig. 7. We have previously described mathematically[1,2] that there is a negative linear relationship between the absorption of the NRs and the scalar orientational order parameter S. As the electric field is increased, the value of S increases from zero for a randomly oriented NR population toward a value of one when the NRs are oriented along the direction of light propagation. The absorption therefore diminishes with increasing field strength in the manner exhibited in Fig. 7. The response is also quantifiable by extracting the critical electric field to align the NRs (E_c), which can be related to geometric and materials parameters.[1,2]

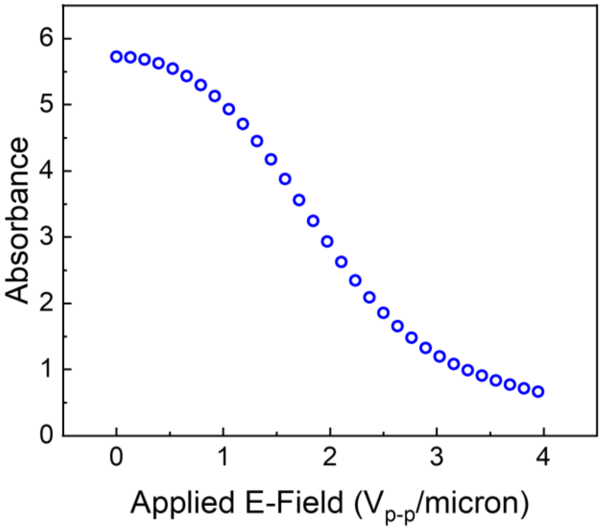

Fig. 7 — Representative measured absorbance at 1064 nm of Au NRs in a pixel cell as a function of applied electric field (E-field). The optical path length in this example is 100 μm, and the applied E-field is estimated by dividing the applied voltage by the distance between the ITO electrodes.

While the principles of alignment behavior noted above had been previously characterized in fairly dilute NR suspensions, here we endeavor to probe NR performance across a wide range of concentrations. The response of pixels prepared with NR suspensions having nominal ODs from 1–10 at a path length of 100 μm is presented in Fig. 8. To provide a comparison with ODs that are commonly quoted for a 1 cm optical path (often used in spectrophotometers), the 1 cm equivalent OD is shown on the right axis of Fig. 8. This scale indicates the absorbance that the NR suspensions in the pixels would have if loaded in a cuvette with an optical path of 1 cm.

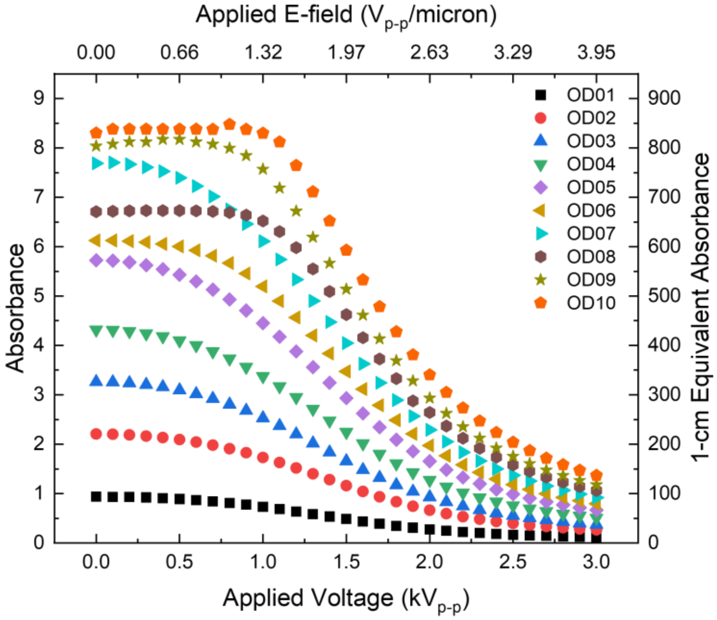

Fig. 8 — Measured absorption at 1064 nm of Au NRs in pixel cells with an optical path of 100 µm as a function of applied voltage (bottom scale) or E-field (top scale). The 1 cm equivalent absorbance (right scale) indicates the absorbance that the NR suspensions in the pixels would have at an optical path of 1 cm. Labels of “OD01–10” indicate nominal optical density targets and represent NR samples prepared with increasing concentrations.

The NR suspensions exhibit the expected alignment behavior over the range of absorbance from ~0–6. Above this range, the trend in absorbance is seen to plateau or saturate. This saturation is clearly visualized in Fig. 9, where absorbance at three different applied voltages is plotted as a function of the NR concentration in the pixels. This plot indicates that the measurement system performs linearly over the ~0–6 OD range, supporting the conclusions from Fig. 8 and setting a reliable range for measurements using this system. The upper limitation on the system’s range is explained by the low light levels at high OD’s reaching the noise floor of the detector, a common feature of absorption measurements. The methods used here are a direct measurement technique but could potentially be expanded to greater ODs using a reference substitution technique employing calibrated optical filters.[10]

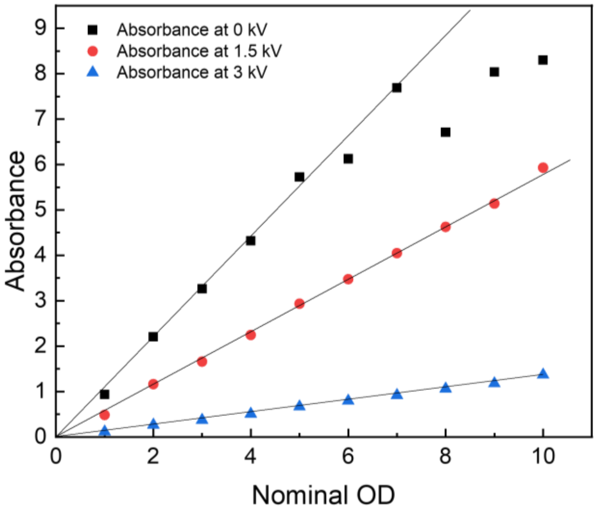

Fig. 9 — Absorbance values at the indicated applied voltage levels extracted from the data of Fig. 8. “Nominal OD” indicates target values used in preparation of the NR suspensions and directly relates to NR concentration. The lines are provided as guides to the eye.

While the concentrations and 1 cm equivalent absorbances of the NR pixels in Fig. 8 are large, we endeavor to expand beyond this range. In order to make direct measurements accessible, the optical path length of the pixels is reduced. Fig. 10 displays the alignment behavior of NR pixels with optical paths of 100, 50, 25, and 10 µm. In each case, NR suspensions are prepared with concentrations that yield absorbance values within the measurable range of 0–6 OD for the given optical path. In order to compare results among the different path lengths, the 1 cm equivalent absorbance values are provided on the right axes of Fig. 10. Notably, the most highly concentrated NR pixel at a path length of 10 µm exhibits a maximum 1 cm equivalent absorbance of nearly 6000 while retaining NR alignment performance.

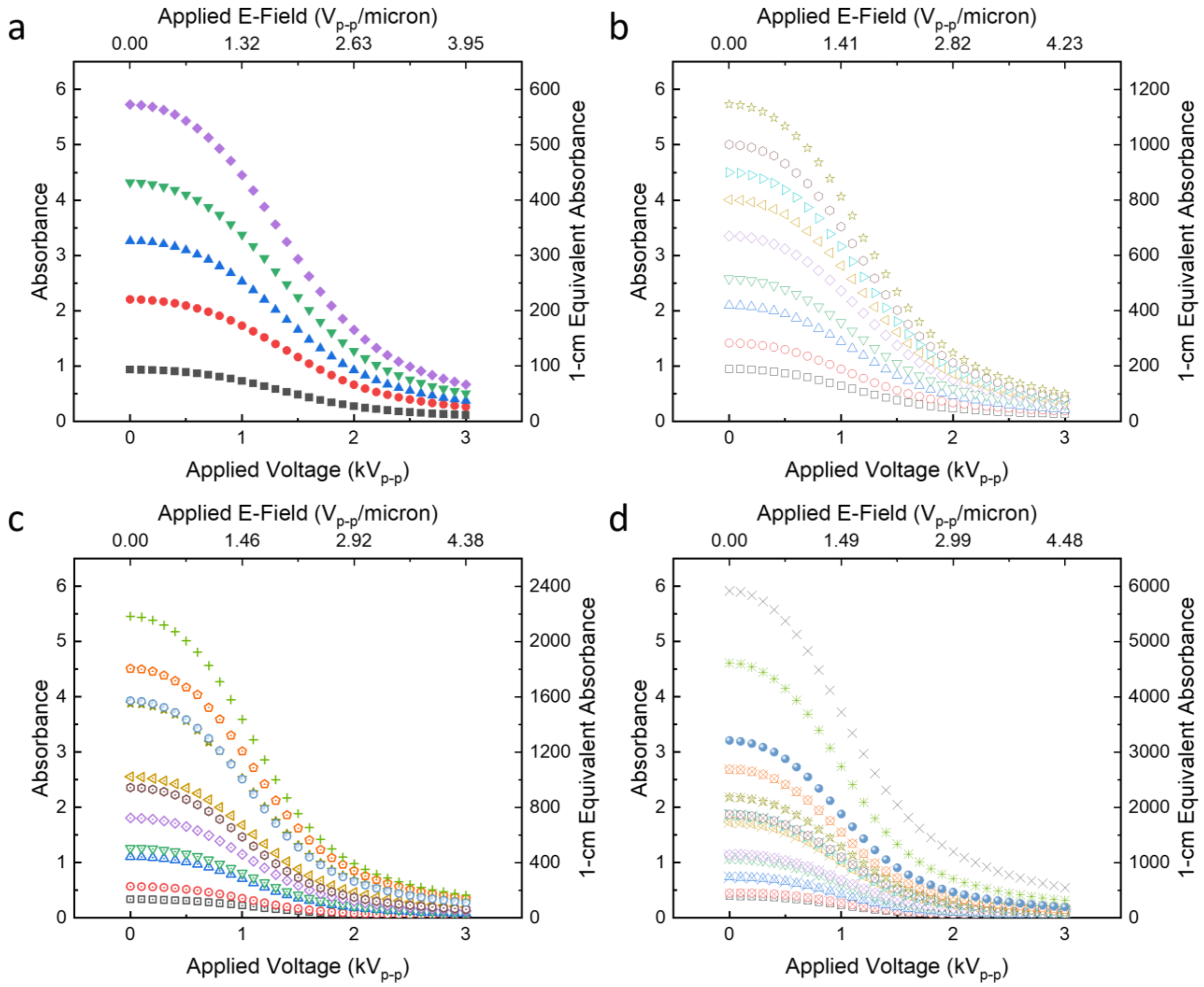

Fig. 10 — Alignment of Au NRs in pixels with optical path lengths of (a) 100 (b) 50 (c) 25 and (d) 10 µm. Individual data sets with unique symbols represent pixels prepared with different concentrations.

The results from all 39 pixels, having among them four different path lengths, are combined into a single plot in Fig. 11a by expressing each data set in terms of 1 cm equivalent absorbance and the geometrically calculated applied electric field strength. Assembled in this manner, the data cover 1 cm equivalent absorbances from 94 to 5916 in the unaligned state, or equivalent transmittances of 10^{-94} to 10^{-5916}. The alignment behavior across this large range (5,822 decades of 1 cm equivalent absorbance) is further assessed by normalizing each pixel's data set to its maximum value, shown in Fig. 11b. Qualitatively, the data across all conditions collapse into a similar function.

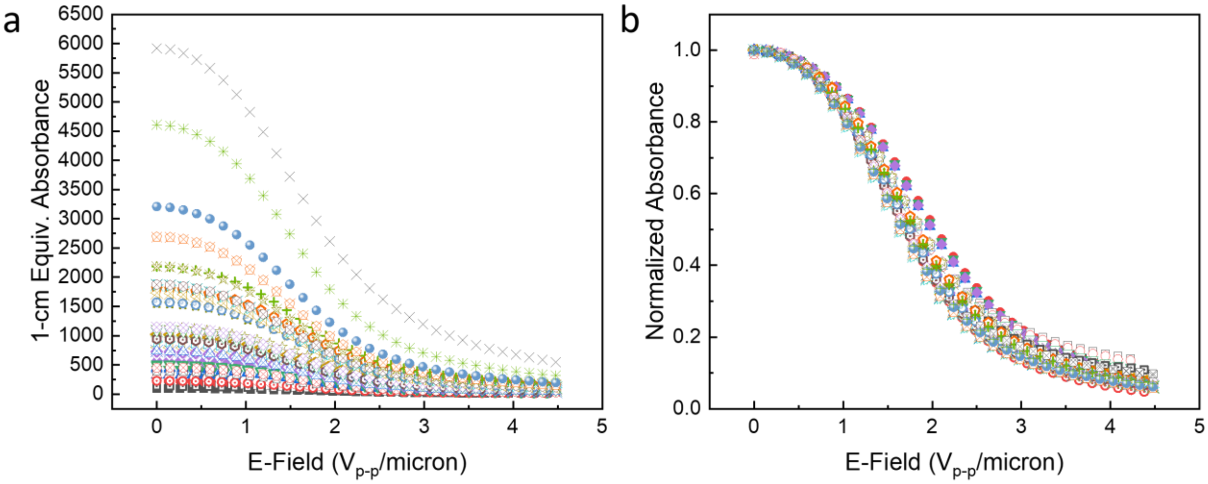

Fig. 11 — (a) Alignment responses of all of the NR pixels (100, 50, 25, and 10 μm paths) from Fig. 10 combined into a single plot expressed in terms of 1 cm equivalent absorbance and geometrically calculated applied electric field strength. (b) Data from (a) where each set is normalized by dividing by its maximum absorbance.

Quantitatively, the data of Fig. 11 are analyzed to extract for each pixel the maximum value of the scalar order parameter S and the critical electric field for alignment E_c, discussed above. The results are shown in Fig. 12, where each pixel is identified by its maximum (unaligned) 1 cm equivalent absorbance value and optical path length. Fig. 12 suggests that the pixels with lesser optical path length achieve a greater degree of NR alignment and align at a lesser electric field strength. Note that the calculated electric field used in the extraction of S and E_c already accounts for the physical difference in spacing between the ITO electrodes in the pixels with different optical path lengths. Finite element method simulations are underway to assess whether this geometric correction adequately describes the electric field distributions in pixels with different electrode spacings.

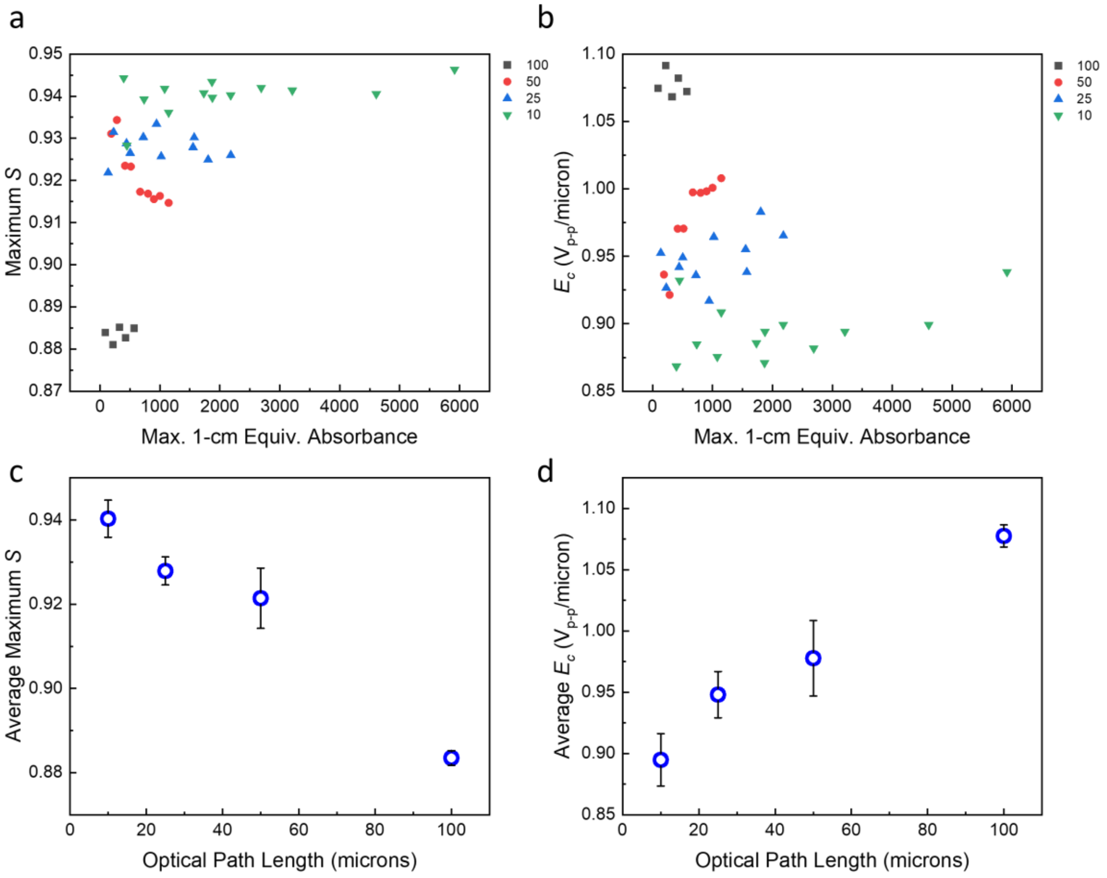

Fig. 12 — (a) Maximum value of the scalar order parameter *S* and (b) value of the critical electric field for alignment E_c extracted from alignment data from pixels with the indicated path lengths (in µm) as a function of the maximum 1 cm equivalent absorbance of the pixel. (c) Average maximum *S* and (d) average E_c for each optical path length, with error bars representing one standard deviation.

Pixel performance is further evaluated by examining the contrast between the pixel on and off states. The absorbance contrast ratio is determined as

$$Absorbance\ contrast\ ratio = \frac{Absorbance_{OFF}}{Absorbance_{ON}} \qquad \text{(Equation 2)}$$

and the transmittance contrast ratio as

$$Transmittance\ contrast\ ratio = \frac{Transmittance_{ON}}{Transmittance_{OFF}} \qquad \text{(Equation 3)}$$

$$= \frac{10^{-Absorbance_{ON}}}{10^{-Absorbance_{OFF}}} = 10^{Absorbance_{OFF} - Absorbance_{ON}} \qquad \text{(Equation 4)}$$

The off state refers to 0 $kV_{p\text{-}p}$ and the on state to 3 $kV_{p\text{-}p}$ applied voltage. The absorbance and transmittance values used in these calculations are the values directly as measured, not the 1 cm equivalent values. The resulting contrast ratios are presented in Fig. 13. The data show that higher absorbance contrast ratios are achieved in thinner pixel cells, with absorbance contrast ratios of at least 15 being consistently achieved. Transmittance contrast ratios of at least 100,000:1 are directly measured for the highest density pixels of all four path lengths.

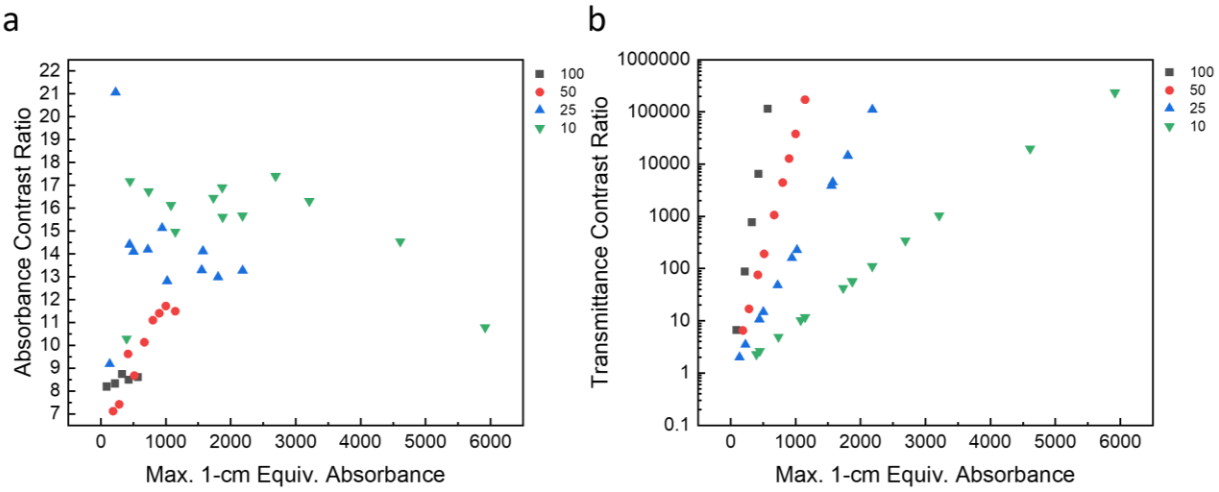

Fig. 13 — (a) Absorbance and (b) transmittance contrast ratio for pixels with the indicated path lengths (in µm) as a function of the maximum 1 cm equivalent absorbance of the pixel

CONCLUSIONS

The fundamental materials properties of Au NR suspensions at exceptionally high NR concentrations and ODs have been uncovered. NR pixels having 1 cm equivalent absorbances of nearly 6000 maintain excellent ability to align under application of electric fields. The highly absorbing pixels consistently display absorbance contrast ratios of at least 15 and transmittance contrast ratios of at least 100,000:1. The materials studied represent the extremes of NR concentration; calculations suggest that the spatial density of NRs within the suspensions approaches the limit that can be supported before NR volumes would overlap. Ongoing work with *in situ* optical microscopy will reveal additional insight on the nature of these phases. Temporally resolved measurements across the concentration ranges studied here may lend further understanding of the dynamics of NR alignment at the extremes of concentration.

The results here reported establish a robust knowledge base for dense plasmonic NR suspensions, vertically integrated from processing, structure, and properties, through to performance in optical applications. This knowledge is foundational for transitioning these materials to impactful innovations. Broadly, it supports the transformation of optical technologies from monolithic and inflexible components toward the agile and adaptable capabilities needed to address an ever-evolving technological environment.

RELATED PUBLICATIONS

Greybush, N. J.; Charipar, K.; Johns, P.; Bauman, S. J.; Doyle, D.; Geldmeier, J.; Naciri, J.; Charipar N.; Fontana, J. Dynamic Plasmonic Nanorod Pixels. In *Proceedings: META 2021, Warsaw – Poland, The 11th International Conference on Metamaterials, Photonic Crystals and Plasmonics*; 2021; pp 466–467.

ACKNOWLEDGEMENTS

The author gratefully acknowledges contributions from Christopher D. Musi, Jawad Naciri, Charles A. Rohde, and Jake Fontana. This work was supported by the Jerome and Isabella Karle Distinguished Scholar Fellowship Program.

REFERENCES

(1) Fontana, J.; Da Costa, G. K. B.; Pereira, J. M.; Naciri, J.; Ratna, B. R.; Palffy-Muhoray, P.; Carvalho, I. C. S. Electric Field Induced Orientational Order of Gold Nanorods in Dilute Organic Suspensions. *Appl. Phys. Lett.* **2016**, *108* (8), 1–5. https://doi.org/10.1063/1.4942969.

(2) Greybush, N. J.; Charipar, K.; Geldmeier, J. A.; Bauman, S. J.; Johns, P.; Naciri, J.; Charipar, N.; Park, K.; Vaia, R. A.; Fontana, J. Dynamic Plasmonic Pixels. *ACS Nano* **2019**, *13* (4), 3875–3883. https://doi.org/10.1021/acsnano.9b00905.

(3) Etcheverry, S.; Araujo, L. F.; Carvalho, I. C. S.; Margulis, W.; Fontana, J. Digital Electric Field Induced Switching of Plasmonic Nanorods Using an Electro-Optic Fluid Fiber. *Appl. Phys. Lett.* **2017**, *111* (22), 221108. https://doi.org/10.1063/1.5001702.

(4) Etcheverry, S.; Araujo, L. F.; da Costa, G. K. B.; Pereira, J. M. B.; Camara, A. R.; Naciri, J.; Ratna, B. R.; Hernández-Romano, I.; de Matos, C. J. S.; Carvalho, I. C. S.; Margulis, W.; Fontana, J. Microsecond Switching of Plasmonic Nanorods in an All-Fiber Optofluidic Component. *Optica* **2017**, *4* (8), 864. https://doi.org/10.1364/OPTICA.4.000864.

(5) Fontana, J.; Greybush, N. J. Plasmonic Nanoparticles as Pixels and Sub-Microsecond Switches. US Patent 10,606,145, 2020.

(6) Nikoobakht, B.; El-Sayed, M. A. Preparation and Growth Mechanism of Gold Nanorods (NRs) Using Seed-Mediated Growth Method. *Chem. Mater.* **2003**, *15* (10), 1957–1962. https://doi.org/10.1021/cm020732l.

(7) Park, K.; Drummy, L. F.; Wadams, R. C.; Koerner, H.; Nepal, D.; Fabris, L.; Vaia, R. A. Growth Mechanism of Gold Nanorods. *Chem. Mater.* **2013**, *25* (4), 555–563. https://doi.org/10.1021/cm303659q.

(8) Park, K. (Manuscript in Preparation).

(9) Guo, Z.; Fan, X.; Xu, L.; Lu, X.; Gu, C.; Bian, Z.; Gu, N.; Zhang, J.; Yang, D. Shape Separation of Colloidal Gold Nanoparticles through Salt-Triggered Selective Precipitation. *Chem. Commun.* **2011**, *47* (14), 4180–4182. https://doi.org/10.1039/c0cc04612d.

(10) Zhang, Z. M.; Gentile, T. R.; Migdall, A. L.; Datla, R. U. Transmittance Measurements for Filters of Optical Density between One and Ten. *Appl. Opt.* **1997**, *36* (34), 8889. https://doi.org/10.1364/ao.36.008889.